

Two-qubit gate operations in superconducting circuits with strong coupling and weak anharmonicity

Xin-You Lü^{1,3}, S. Ashhab^{1,2}, Wei Cui¹, Rebing Wu^{1,4}, and Franco Nori^{1,2}

¹*Advanced Science Institute, RIKEN,
Wako-shi, Saitama 351-0198, Japan*

²*Physics Department, The University of Michigan,
Ann Arbor, Michigan 48109-1040, USA*

³*School of Physics, Ludong University, Yantai 264025, P. R. China*

⁴*Department of Automation, Center for Quantum information Science and Technology,
Tsinghua University, Beijing, 100084, P.R. China*

(Dated: September 2, 2022)

Abstract

We investigate theoretically the implementation of two-qubit gates in a system of two coupled superconducting qubits. In particular, we analyze two-qubit gate operations under the condition that the coupling strength is comparable to or even larger than the anharmonicity of the qubits. By numerically solving the time-dependent Schrödinger equation, we obtain the dependence of the two-qubit gate fidelity on the system parameters in the case of direct and indirect qubit-qubit coupling. Our numerical results can be used to identify the “safe” parameter regime for experimentally implementing two-qubit gates with high fidelity in these systems.

PACS numbers: 03.67.-a; 42.50.Pq; 85.25.-j

I. INTRODUCTION

Superconducting circuits (SC) based on Josephson junctions are promising candidates for the realization of scalable quantum computing on a solid-state platform, due to their design flexibility, large-scale integration and controllability (see the reviews in Refs. [1–7]). Superconducting qubits include the charge [8], flux [9], and phase qubits [10] as well as their variants, capacitively shunted flux qubits [11] and capacitively shunted charge qubits (transmon) [12]. The phase qubit, the capacitively shunted flux qubit and the transmon qubit are relatively insensitive to charge noise and can be operated over a wide range of parameters. Single-qubit gates [13], two-qubits gates [14, 15] and simple quantum algorithms [16] with superconducting qubits have been demonstrated experimentally in recent years. However, the common disadvantage of these types of qubits is their weakly anharmonic energy level structure, i.e., the detuning between adjacent transition frequencies is very small.

Generally, the influence of the small anharmonicity (denoted by Δ) on quantum gate operations can be neglected when the qubit-field or qubit-qubit coupling strength is very small compared with Δ . However, for the practical application of quantum computation, one wants to maximize the number of quantum gate operations with a given coherence time. In other words, we must implement quantum operations as fast as possible, which requires a strong qubit-qubit or qubit-field coupling to be employed during the single- and two-qubit gate operations. The anharmonicity of phase or transmon qubits will influence the quality of quantum gates more and more with increasing coupling strength. Recently, there have been a number of theoretical studies analyzing the effects of weak anharmonicity of superconducting qubits on the operation of single-qubit gates and several optimization strategies have been proposed based on varying driving pulse shapes and pulse sequences [17–21].

The influence of weak anharmonicity on single-qubit gate operations mainly comes from direct transitions from qubit states (two lowest energy levels) to higher excited states, and its basic principle can be illustrated using the Bloch sphere (see Fig. 1). Suppose a three-level system interacts with a classical or quantum field with coupling strength g . The lowest two states, $|g\rangle$ and $|e\rangle$, comprise the qubit subspace, $|a\rangle$ is the third level, and Δ denotes the anharmonicity. The transition between the two qubit states corresponds to a rotation

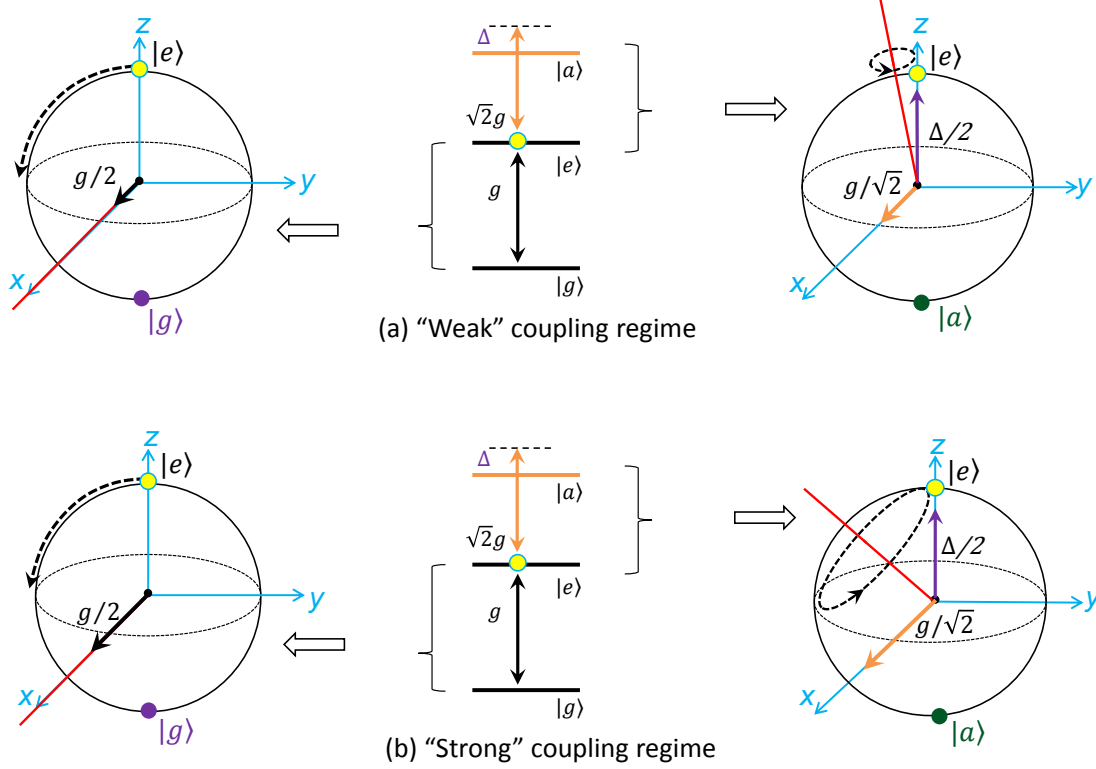


FIG. 1: (Color online) A simplified Bloch-sphere representation of the transitions $|g\rangle \leftrightarrow |e\rangle$ and $|e\rangle \leftrightarrow |a\rangle$ in the “weak” coupling regime (a) and the “strong” coupling regime (b). The transition between different states correspond to rotations about the corresponding axes of rotations (red lines). In the two Bloch spheres on the left, the length of the black arrows along the x -axis denote the coupling strength $g/2$. These are shown as orange arrows along the x -axis, in the two Bloch spheres on the right, but now with magnitude $\sqrt{2}g/2$ instead of $g/2$. The coordinate axes (x, y, z) are shown in blue.

about some axis (red line in Fig. 1) in the Bloch sphere. When a driving field resonant with the $|e\rangle \leftrightarrow |g\rangle$ transition, the transition $|e\rangle \leftrightarrow |a\rangle$ will be driven with detuning Δ . As shown in Figs. 1(a) and (b), the transition between $|e\rangle$ and $|a\rangle$ can be neglected in the “weak” coupling regime, whereas we must take into consideration such transitions in the “strong” coupling regime. Here, “weak” coupling means that the qubit-field coupling strength $g \ll \Delta$, while “strong” coupling means that g is comparable to or even larger than Δ .

Similar to single-qubit gates, the weak anharmonicity of superconducting qubits will also influence the implementation of two-qubit gates. Then two questions arise naturally: (1) how much the weak anharmonicity of the qubits influence the implementation of two-

qubit gates in a system of coupled superconducting qubits? (2) how strong can the coupling be while allowing a high two-qubit gate fidelity? In other words, how fast can two-qubit gates with high fidelity be implemented, given the weak anharmonicity of superconducting qubits?

Motivated by the above questions, in this paper we study the implementation of two-qubit gates with SC systems in the “strong” coupling regime. We numerically simulate the influence of the coupling strength and anharmonicity on the fidelities of two-qubit gates in different SC systems, and provide some general conclusions. Based on our numerical results, the “safe” parameter regime for implementing two-qubit gates with high fidelity is identified, which can be used to guide experimental efforts based on superconducting qubits. The remainder of this paper is organized into four parts as follows. In section II, we introduce some possible methods for implementing two-qubit gates and qualitatively discuss the effect of strong coupling. In section III, we present results of numerical calculations that demonstrate the influence of the corresponding coupling strength and anharmonicity on the performance of two-qubit gates, and then identify the “safe” parameter regime for implementing two-qubit gates with high fidelity. Finally, we conclude with a brief summary in section IV.

II. MODEL AND QUALITATIVE DISCUSSION

In this section, we will describe possible methods for the implementation of two-qubit gates in circuits with direct and indirect qubit-qubit coupling. By qualitatively analyzing the influence of the qubit-qubit (or qubit-cavity) coupling strength and the anharmonicity of the superconducting qubits on the two-qubit gate, we obtain some general conclusions about the quality of two-qubit gates with superconducting-qubit systems in the “strong” coupling regime.

A. System with direct qubit-qubit coupling

As shown in Fig. 2(a), as a model system we consider two capacitively coupled superconducting phase qubits. The weakly-anharmonic multilevel structure of each phase qubit is presented in Fig. 2(b). The two lowest levels $\{|0\rangle_j, |1\rangle_j\}$, separated in energy by $\hbar\omega_j$

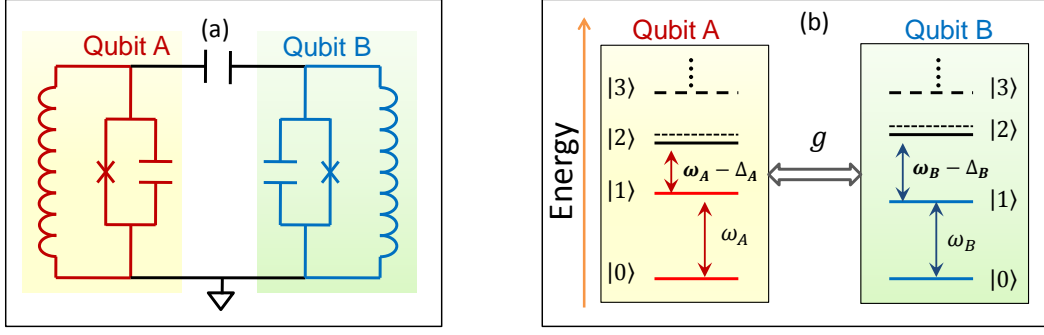


FIG. 2: (Color online) (a) Circuit diagram for capacitively coupled flux-biased phase qubits. (b) Energy-level diagrams for the qubits. g and Δ_j ($j = A, B$) are the coupling strength and anharmonicity, respectively.

($j = A, B$), are the computational basis, and the n th ($n \geq 2$) higher levels are different from $n\hbar\omega_j$ by $\hbar\epsilon_n^j$. Here ϵ_n^j has the standard nonlinear oscillator form $\epsilon_n^j = \Delta_j(n-1)n/2$ [22] and Δ_j is the anharmonicity of the qubit, and it is positive in our paper. The Hamiltonian of the coupled system is given by ($\hbar = 1$) [23–27]

$$H = \sum_{n=1}^{N-1} [(n\omega_A - \epsilon_n^A) |n\rangle_A \langle n| + (n\omega_B - \epsilon_n^B) |n\rangle_B \langle n|] + gJ_A^x \otimes J_B^x, \quad (1a)$$

$$J_A^x = \sum_{n=1}^{N-1} \eta_{n-1,n}^A \sigma_{n-1,n}^{Ax}, \quad J_B^x = \sum_{n=1}^{N-1} \eta_{n-1,n}^B \sigma_{n-1,n}^{Bx}, \quad (1b)$$

where N is the number of levels in each superconducting qubit, $\eta_{n-1,n}^j = \sqrt{n}$ is the level-dependent coupling matrix element, and $\sigma_{n-1,n}^{jx} = |n-1\rangle_j \langle n| + |n-1\rangle_j \langle n|$ is the effective Pauli spin operators for levels $|n-1\rangle$ and $|n\rangle$. Also, g denotes the qubit-qubit coupling strength.

In order to qualitatively analyze the implementation and fidelity of two-qubit gates, we assume in this subsection that each phase qubit has three levels. Then, in the interaction picture, the interaction Hamiltonian of the coupled system, under the rotation-wave approximation (RWA), can be reduced to

$$H_I = g[|01\rangle \langle 10| e^{i(\omega_B - \omega_A)t} + \sqrt{2}|02\rangle \langle 11| e^{i(\omega_B - \omega_A - \Delta_B)t} + \sqrt{2}|20\rangle \langle 11| e^{i(\omega_A - \omega_B - \Delta_A)t} + 2|12\rangle \langle 21| e^{i(\omega_B - \omega_A - \Delta_B + \Delta_A)t} + h.c.], \quad (2)$$

where $|mn\rangle$ denotes $|m\rangle_A |n\rangle_B$.

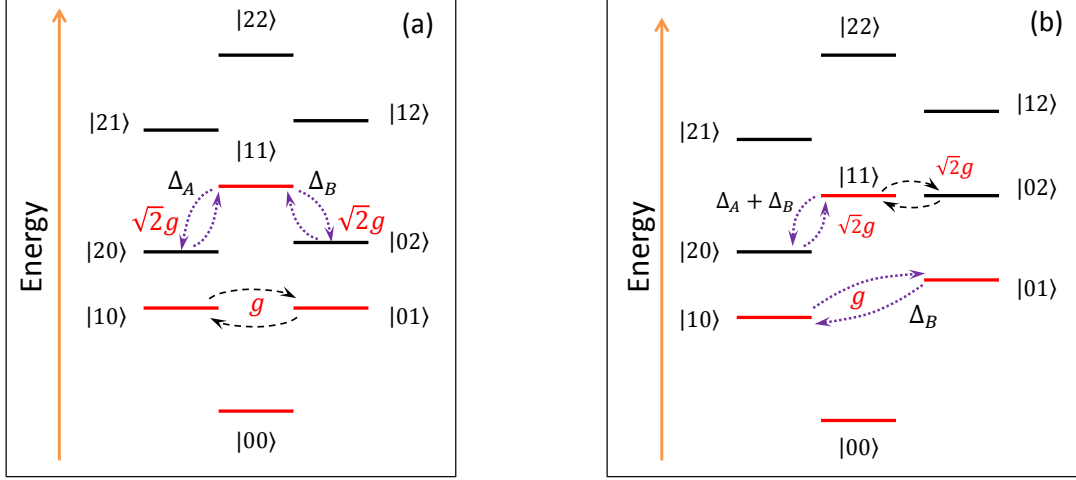


FIG. 3: (Color online) The energy-level diagram of two-qubit product states for the iSWAP gate (a), and the controlled-Z gate (b). Red levels denote the states in the computational basis. The black dashed arrows are the resonant transitions used for realizing the two-qubit gates and the purple dotted arrows are the main *undesired* transitions, which adversely affect the implementation of two-qubit gates.

From the above Hamiltonian, it is easily seen that we can obtain different resonant transitions by appropriately adjusting the qubit frequencies, ω_A and ω_B , and then realize various two-qubit gates after a properly chosen interaction time. For example, in the weak-coupling regime $g \ll |\Delta_j|$, the two-qubit iSWAP [14] and CZ [15] gates have been implemented experimentally with high fidelity based on the above picture. A natural question is whether the two-qubit gate can still be realized with high fidelity with larger coupling strengths g . Next, we will discuss in detail the implementation and quality of two-qubit iSWAP and CZ gates in the strong-coupling regime, where the corresponding coupling strength is comparable to or even larger than the anharmonicity of the superconducting qubit.

1. Two-qubit iSWAP gate

The key for implementing the two-qubit iSWAP gate is the resonant transition between the states $|01\rangle$ and $|10\rangle$, which can be realized by setting $\omega_A = \omega_B$. Under this condition, we plot the energy-level diagram of the product state basis and the interaction-induced couplings in Fig. 3(a). The states $|00\rangle$, $|01\rangle$, $|10\rangle$, and $|11\rangle$ are the two-qubit computational

basis. From Fig. 3(a), it can be seen that apart from the resonant transition $|01\rangle \leftrightarrow |10\rangle$, there are also two main undesired transitions, $|11\rangle \leftrightarrow |02\rangle$ and $|11\rangle \leftrightarrow |20\rangle$, with strength $\sqrt{2}ge^{-i\Delta_j t}$ ($j = A, B$), which will influence the implementation of the quantum gate.

As shown in the experimental method [14], in the weak-coupling limit, $g \ll |\Delta_j|$, the above two undesired transitions have average amplitude $g/|\Delta_j|$ and can be safely ignored. Then, for an interaction time $gt_g = \pi/2$, the iSWAP gate is realized with high fidelity, i.e., $|00\rangle \rightarrow |00\rangle$, $|01\rangle \rightarrow -i|10\rangle$, $|10\rangle \rightarrow -i|01\rangle$, $|11\rangle \rightarrow |11\rangle$. However, with increasing coupling strength g , the strengths of the transitions $|11\rangle \rightarrow |02\rangle$, and $|11\rangle \rightarrow |20\rangle$ become larger and larger. In other words, the influence of the undesired transitions on the two-qubit iSWAP gate cannot be safely ignored when the anharmonicity of the qubit is not much larger than the coupling strength g . From the above qualitative discussion, we can obtain a simple conclusion: the relative value of the coupling strength g and the anharmonicity Δ_j is an important parameter for the quality of the two-qubit iSWAP gate.

2. Two-qubit CZ gate

The key for implementing the two-qubit CZ gate following Ref. [28] is the resonant transition between the states $|11\rangle$ and $|02\rangle$, which can be realized by setting $\omega_B = \omega_A + \Delta_B$. Under this condition, we plot the energy-level diagram of the product state basis and the interaction-induced couplings in Fig. 3(b). It is easily found from Fig. 3(b) that there are also two main undesired transitions, $|11\rangle \leftrightarrow |20\rangle$ and $|01\rangle \leftrightarrow |10\rangle$, which will influence the quality of two-qubit CZ gate.

As shown in the experimental method [15], in the weak-coupling regime, $g/\Delta_A, g/\Delta_B \ll 1$, the transitions $|11\rangle \leftrightarrow |20\rangle$ and $|01\rangle \leftrightarrow |10\rangle$, with respective average strengths $\sqrt{2}g/(\Delta_A + \Delta_B)$ and g/Δ_B , can be safely ignored and the two-qubit CZ gate is realized with high fidelity after an interaction time $\sqrt{2}gt = \pi$, i.e. $|00\rangle \rightarrow |00\rangle$, $|01\rangle \rightarrow |01\rangle$, $|10\rangle \rightarrow |10\rangle$, $|11\rangle \rightarrow -|11\rangle$. However, with increasing coupling strength g , the undesired transitions $|11\rangle \leftrightarrow |20\rangle$ and $|01\rangle \leftrightarrow |10\rangle$ cannot be safely ignored any more, and they will reduce the fidelity of the two-qubit CZ gate. So, once again $g/|\Delta_j|$ is an important parameter for the quality of the two-qubit CZ gate, and strong-coupling will lead to a reduced fidelity of the quantum gate.

B. System with indirect qubit-qubit coupling

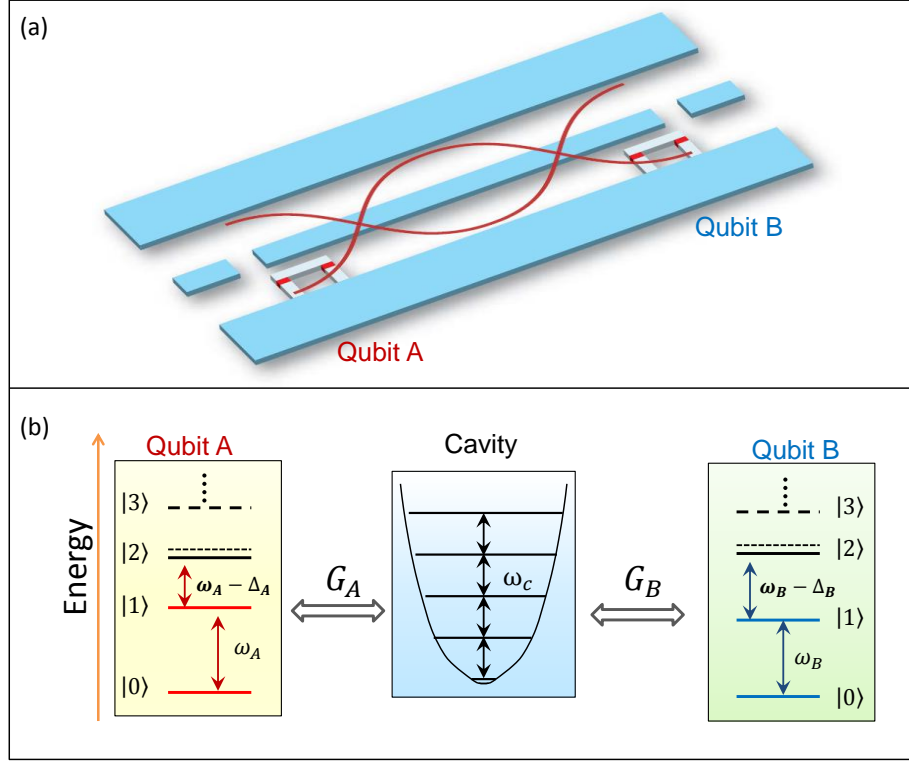


FIG. 4: (Color online). (a) Schematic diagram of an experimental setup of a system with indirect qubit-qubit coupling for implementing two-qubit gates. Two transmons are fabricated inside a transmission line resonator and interact indirectly via the common quantized field. (b) Energy-level diagrams for the transmons and the cavity. Here G_j and Δ_j ($j = A, B$) are the qubit-cavity coupling strengths and anharmonicity of the qubits, respectively.

As shown in Fig. 4(a), the model considered here is two transmons capacitively coupled to a common transmission line resonator. Each transmon has a weakly anharmonic multilevel structure [see Fig. 4(b)]. Similar to the phase qubit, the two lowest levels separated by $\hbar\omega_j$ define the qubit subspace, and the higher levels are different from $n\hbar\omega_j$ by $\hbar\epsilon_n^j$. The Hamiltonian of the coupled system is given by

$$H = \omega_c a^\dagger a + \sum_{j=A,B} \left[\sum_{n=1}^{N-1} (n\omega_j - \epsilon_n^j) |n\rangle_j \langle n| + G_j (a + a^\dagger) J_j^x \right], \quad (3)$$

where ω_c is the frequency of the quantized cavity mode; and G_j denotes the coupling strength between qubit j and the cavity mode. The definitions of the other parameters are the same

as in Eq. (1). Under the rotation-wave approximation and considering each transmon with three levels, the Hamiltonian (3) can be reduced to

$$H = H_0 + H_I, \quad (4a)$$

$$H_0 = \omega_c a^\dagger a + \sum_{j=A,B} [\omega_j |1\rangle_j \langle 1| + (2\omega_j - \Delta_j) |2\rangle_j \langle 2|], \quad (4b)$$

$$H_I \approx \sum_{j=A,B} \left(G_j a^\dagger |0\rangle_j \langle 1| + \sqrt{2} G_j a^\dagger |1\rangle_j \langle 2| + h.c. \right). \quad (4c)$$

In this system with indirect qubit-qubit coupling, an effective qubit-qubit coupling can be realized via two types of qubit-cavity interactions: dispersive interaction and resonant interaction. Next, we will discuss the implementation and quality of two different two-qubit gates based on the above approaches.

1. Dispersive qubit-cavity interaction approach

In the dispersive qubit-cavity-coupling approach, the cavity mode is off-resonant with the qubit transition frequency, i.e., $|\delta_j| = |\omega_j - \omega_c| \gg G_j$ ($j = A, B$), and the qubits exchange energy by virtual photon processes. Then, the Hamiltonian (4) can be transformed to an effective Hamiltonian by a Fröhlich transformation [29–32],

$$\begin{aligned} H_{\text{eff}} &= e^{-S} H e^S \\ &\approx \sum_{j=A,B} \left\{ \left[\left(\omega_j + \frac{G^2}{\delta_j} \right) |1\rangle_j \langle 1| + \left(2\omega_j - \Delta_j + \frac{2G^2}{\delta_j - \Delta_j} \right) |2\rangle_j \langle 2| + \frac{G^2}{2\delta_j} a^\dagger a (|1\rangle_j \langle 1| - |0\rangle_j \langle 0|) \right. \right. \\ &\quad \left. \left. + \frac{G^2}{\delta_j - \Delta_j} a^\dagger a (|2\rangle_j \langle 2| - |1\rangle_j \langle 1|) \right] + \left[\frac{\sqrt{2}G^2}{2} \left(\frac{1}{\delta_j - \Delta_j} - \frac{1}{\delta_j} \right) a^2 |2\rangle_j \langle 0| \right. \right. \\ &\quad \left. \left. + \frac{G^2}{2} \left(\frac{1}{\delta_A} + \frac{1}{\delta_B} \right) |01\rangle \langle 10| + \frac{\sqrt{2}G^2}{2} \left(\frac{1}{\delta_B - \Delta_B} + \frac{1}{\delta_A} \right) |02\rangle \langle 11| \right. \right. \\ &\quad \left. \left. + \frac{\sqrt{2}G^2}{2} \left(\frac{1}{\delta_A - \Delta_A} + \frac{1}{\delta_B} \right) |20\rangle \langle 11| + G^2 \left(\frac{1}{\delta_A - \Delta_A} + \frac{1}{\delta_B - \Delta_B} \right) |12\rangle \langle 21| + h.c. \right] \right\}, \quad (5) \end{aligned}$$

where

$$S = \sum_{j=A,B} \left[\frac{G}{\delta_j} a^\dagger |0\rangle_j \langle 1| + \frac{\sqrt{2}G}{\delta_A - \Delta_A} a^\dagger |1\rangle_j \langle 2| - h.c. \right]. \quad (6)$$

Here, we have assumed that $G_A = G_B = G$.

Assuming the quantized cavity mode to initially be in the vacuum state and neglecting the field-induced level shifts and two-photon processes, the Hamiltonian (7) can be simplified further as

$$H'_{\text{eff}} = \left[\sqrt{2}g_{\text{eff1}}|02\rangle\langle 11|e^{i(\omega_B-\omega_A-\Delta_B)t} + \sqrt{2}g_{\text{eff2}}|20\rangle\langle 11|e^{i(\omega_A-\omega_B-\Delta_A)t} \right. \\ \left. + g_{\text{eff3}}|01\rangle\langle 10|e^{i(\omega_B-\omega_A)t} + 2g_{\text{eff4}}|12\rangle\langle 21|e^{i(\omega_B-\omega_A-\Delta_B+\Delta_A)t} + h.c. \right]. \quad (7)$$

where $g_{\text{eff1}} = \frac{G^2}{2}(\frac{1}{\delta_B-\Delta_B} + \frac{1}{\delta_A})$, $g_{\text{eff2}} = \frac{G^2}{2}(\frac{1}{\delta_A-\Delta_A} + \frac{1}{\delta_B})$, $g_{\text{eff3}} = \frac{G^2}{2}(\frac{1}{\delta_A} + \frac{1}{\delta_B})$, $g_{\text{eff4}} = \frac{G^2}{2}(\frac{1}{\delta_A-\Delta_A} + \frac{1}{\delta_B-\Delta_B})$. Now, we obtain an effective interaction Hamiltonian similar to the Hamiltonian (2) in the system with direct qubit-qubit coupling. So, in principle, the two-qubit iSWAP and CZ gates can be realized in the dispersively coupled system by adjusting the qubit frequencies. For example, the two-qubit CZ gate has been implemented experimentally based on the above approach [16]. In the experiment [16], the weak-coupling condition $g_{\text{effm}} \ll |\Delta_j|$ ($m = 1 - 4; j = A, B$) is still required for ignoring the influence of the undesired transitions $|01\rangle \leftrightarrow |10\rangle$ and $|20\rangle \leftrightarrow |11\rangle$, and obtaining a high-fidelity two-qubit CZ gate. Here g_{effm} is the effective qubit-qubit coupling strength and $g_{\text{effm}} \propto G^2/\delta_j$. So, when the qubit-cavity detuning δ_j is fixed, with increasing coupling strength G , the effective qubit-qubit coupling will be close to or even larger than the anharmonicity of the qubits Δ_j ($j = A, B$). Then the influence of the undesired transitions $|01\rangle \leftrightarrow |10\rangle$ and $|20\rangle \leftrightarrow |11\rangle$ on the two-qubit CZ gate cannot be ignored any more. As a result, in the dispersive qubit-cavity interaction method, the relative value of g_{effm} and Δ_j can be used to evaluate the fidelity of two-qubit CZ gate. Strong-coupling regime, where g_{effm} is comparable to or larger than Δ_j , will lead to a reduced fidelity. Of course, the above conclusion is also valid for the two-qubit iSWAP gate.

2. Resonant qubit-cavity interaction approach

In the resonant qubit-cavity-coupling approach, the cavity mode frequency can be tuned to switch selectively on and off its resonant coupling to the qubits [33]. As shown in [34] and Fig. 5, the two-qubit CZ gate can be realized via a three-step qubit-field resonant interaction. Here, the first and third steps are two mapping processes between qubit A and the cavity through resonant coupling, and under the RWA there is no undesired transition influencing the mapping processes. So the mapping processes will be realized ideally regardless of the

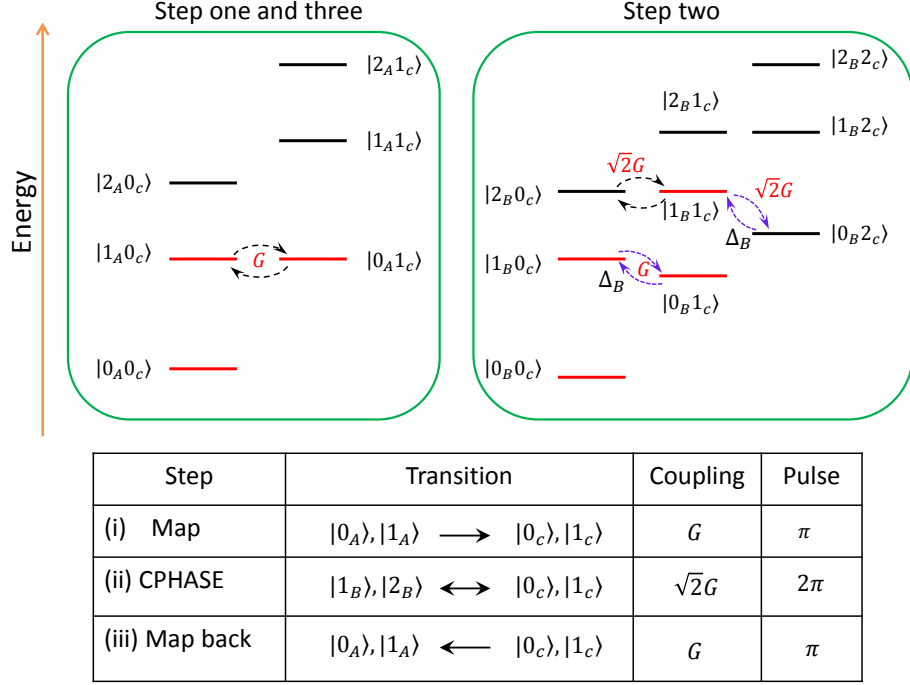


FIG. 5: (Color online) The energy-level diagram and protocol for the two-qubit CZ gate in the resonant qubit-cavity coupling approach [34]. The black dashed arrows are the resonant transitions for realizing the two-qubit gate and the blue dotted arrows are the main *undesired* transition, which influence the two-qubit gate.

coupling strength. In the second step, there are two undesired transitions, $|1_B 0_c\rangle \leftrightarrow |0_B 1_c\rangle$ and $|1_B 1_c\rangle \leftrightarrow |0_B 2_c\rangle$, influencing the “CPHASE” process, and hence the weak-coupling condition, $G \ll \Delta_B$, was assumed in Ref. [34] in order to ignore the influence of the above two undesired transitions and obtain high-fidelity two-qubit gates. However, with increasing coupling strength G , the average strengths of the above two transitions will become larger and larger. So, the undesired transitions cannot be neglected any more in the strong-coupling regime, which will lead a reduced fidelity of quantum gate operations.

Before ending this section, we would like to give a general conclusion from the above qualitative discussion. Both in the cases of direct and indirect qubit-qubit coupling, the fidelity of the two-qubit gates is mainly decided by the relative value of the qubit-qubit or qubit-cavity coupling strength and the anharmonicity of the qubits. The fidelity of the two-qubit gate will decrease with increasing g/Δ_j , g_{effm}/Δ_j , or G/Δ_j . So, in the two-qubit gate approach based on superconducting qubits, a very strong qubit-qubit or cavity-qubit

coupling strength cannot be employed due to the weak anharmonicity of the qubits, if one wants to obtain a high fidelity. How strong the coupling can be, while allowing high two-qubit-gate fidelities, will be analyzed in detail in the next section.

III. NUMERICAL RESULTS

In this section, we will numerically calculate the fidelity of two-qubit gates in the circuits with either direct or indirect qubit-qubit coupling. Importantly, the present numerical results can help identify the safe parameter regime for implementing two-qubit gates with high fidelity.

Here, the fidelity of a two-qubit gate is defined as the Euclidean distance between the target U_T and the actual evolution $U(t_g)$ [20],

$$F = 1 - \frac{1}{16} \|U_T - P^\dagger U(t_g) P\|_2^2, \quad (8)$$

where $U(t)$ is the usual time evolution operator obeying the Schrödinger equation $\dot{U}(t) = -\frac{i}{\hbar} H(t) U(t)$ in the full space of the quantum system. Here $\|X\|_2^2 = \text{tr}(X^\dagger X)$ where X is an arbitrary operator. P is the projection operator on the two-qubit computational $\{|00\rangle, |01\rangle, |10\rangle, |11\rangle\}$; $U_T = |00\rangle\langle 00| - i|01\rangle\langle 10| - i|10\rangle\langle 01| + |11\rangle\langle 11|$ corresponds to the two-qubit iSWAP gate, and $U_T = |00\rangle\langle 00| + |01\rangle\langle 01| + |10\rangle\langle 10| - |11\rangle\langle 11|$ corresponds to the two-qubit CZ gate. Here it should be pointed out that single-qubit rotations and an overall phase factor $U_z^A = e^{i\theta_A \sigma_z^A}$, $U_z^B = e^{i\theta_B \sigma_z^B}$, $U_I = e^{i\theta I}$ are used in the numerical calculations in order to eliminate any extra phase factors. Also, I is the unit matrix and $\sigma_z^A = |00\rangle\langle 00| + |01\rangle\langle 01| - |10\rangle\langle 10| - |11\rangle\langle 11|$, $\sigma_z^B = |00\rangle\langle 00| - |01\rangle\langle 01| + |10\rangle\langle 10| - |11\rangle\langle 11|$. Moreover, θ_A , θ_B and θ are arbitrary arguments chosen in order to maximize the fidelity.

A. System with direct qubit-qubit coupling

In section II, we have qualitatively discussed the performance of two-qubit gates in a circuit with direct qubit-qubit coupling. In this subsection, based on the original Hamiltonian (2), we numerically calculate the influence of the coupling strength g and anharmonicity Δ_j on the fidelities of the two-qubit iSWAP and CZ gates (see Figs. 6-10). Here we consider the two-qubit iSWAP and CZ gates implemented in the experimental methods [14] and [15], and all the parameters used in the numerical calculations are consistent with these experiments.

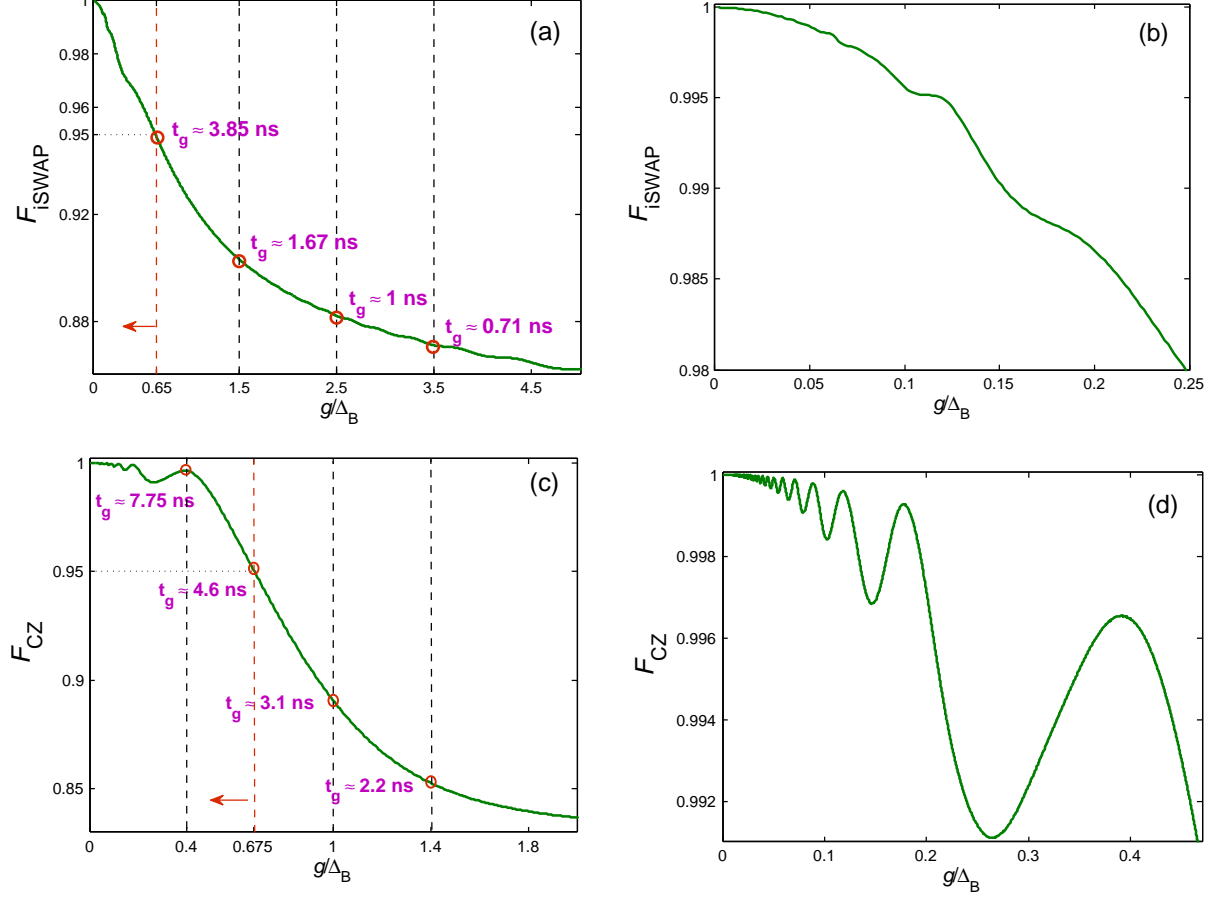


FIG. 6: (Color online) The fidelities of the two-qubit iSWAP gate F_{iSWAP} in (a) and (b); and F_{iSWAP} CZ gate (c), (d); as functions of g/Δ_B in a circuit with direct qubit-qubit coupling. In figures (a) and (c), some representative dots are denoted by the dashed lines and red circles in order to present the relationship between the gate time t_g and fidelity F . The red arrows point out the parameter regime corresponding to two-qubit gate fidelities higher than 95%. In figures (b) and (d), we plot the high-fidelity parts of (a) and (c). The system parameters used here are: (a), (b) $\omega_A/2\pi = 5.5$ GHz, $\omega_B = \omega_A$, $\Delta_A/2\pi = 0.15$ GHz, and $\Delta_B/2\pi = 0.1$ GHz; (c), (d) $\omega_A/2\pi = 7.16$ GHz, $\Delta_A/2\pi = 0.087$ GHz, $\Delta_B/2\pi = 0.114$ GHz, and $\omega_B = \omega_A + \Delta_B$.

In Figs. 6(a) and (c), we plot the fidelities of the two-qubit iSWAP gate (F_{iSWAP}) and the CZ gate (F_{CZ}) as functions of g/Δ_B in a circuit with direct qubit-qubit coupling, where we consider each superconducting qubit to have three levels (same approximation will be used in Figs. 7-9). From Figs. 6(a) and (c), it can be seen that the two-qubit iSWAP and CZ gates can be realized with high fidelities under the condition $g/\Delta_B \ll 1$, which is consistent

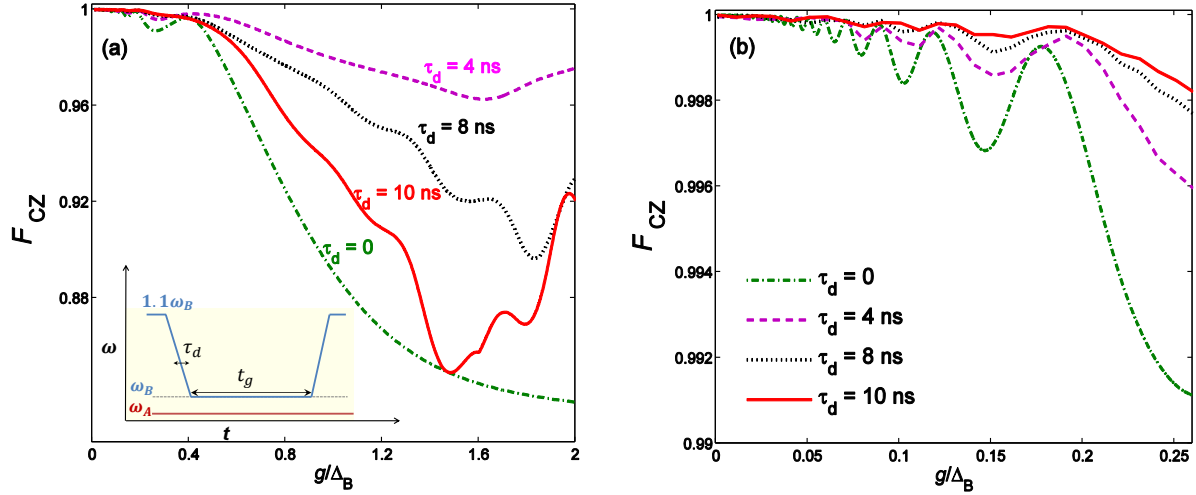


FIG. 7: (Color online) (a) The fidelity F_{CZ} of the two-qubit CZ gate as a function of g/Δ_B in a circuit with direct qubit-qubit coupling, where the qubit frequencies are adiabatically adjusted during the gate operation. (b) The high-fidelity part of (a). As shown in the inset of (a), the frequency of qubit B starts at $1.1\omega_B$, is first ramped down to ω_B in a period of time τ_d , then ramped up to $1.1\omega_B$ after an interaction time t_g ($\sqrt{2}gt_g = \pi$). The system parameters are the same as in Fig. 6(c).

with the experimental results in Refs. [14] and [15]. However, the fidelities of these gates decrease with increasing g/Δ_B . The present numerical results can help identify the safe parameter regime for realizing two-qubit gates with high fidelities. As shown in Figs. 6(a) and (c), if we want to implement the two-qubit iSWAP (CZ) gate with fidelity higher than 95%, the safe parameter regime is $g/\Delta_B < 0.65$ ($g/\Delta_B < 0.675$). In other words, based on the relationship $gt_g = \pi/2$ for the iSWAP gate and $\sqrt{2}gt_g = \pi$ for the CZ gate, the present numerical results can also identify the time limit for implementing two-qubit gates with high fidelity. For example, here the shortest gate time is $t_g \approx 3.85$ ns ($t_g \approx 4.6$ ns) for implementing a two-qubit iSWAP (CZ) gate with fidelity higher than 95%, as shown in Figs. 6(a) and (c). In addition, we individually present the high-fidelity parts of Figs. 6(a) and (c) in the Figs. 6(b) and (d), which is important to guide new two- and multi-qubit experiments using high-fidelity quantum gates.

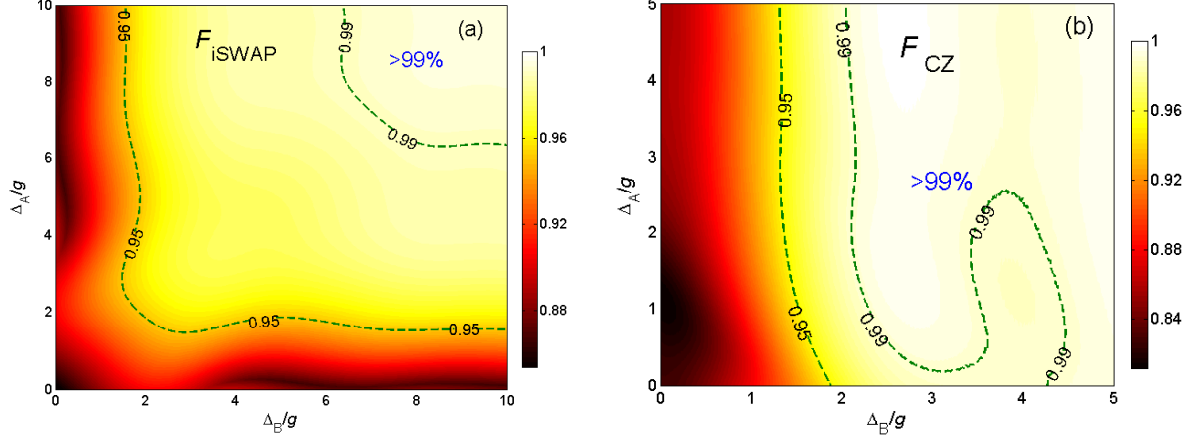


FIG. 8: (Color online) The fidelities of the two-qubit iSWAP gate (a) F_{iSWAP} and CZ gate F_{CZ} (b) versus Δ_A/g and Δ_B/g in a circuit with direct qubit-qubit coupling. The dashed lines correspond to the parameter regime for implementing a two-qubit gate with fidelities 95% and 99%. The system parameters are the same as in Fig.6 except for $g/2\pi = 0.2$ GHz

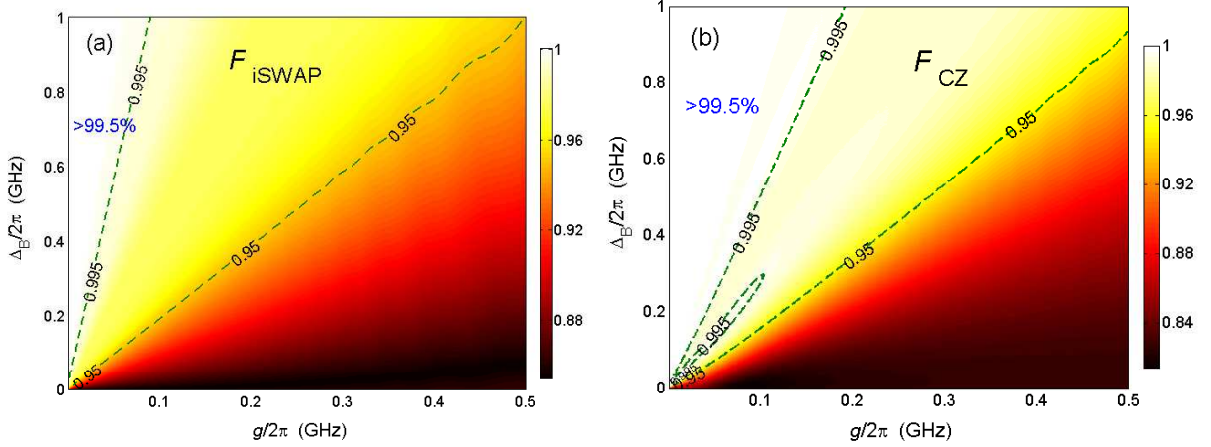


FIG. 9: (Color online) The fidelities of the two-qubit iSWAP (a) and CZ (b) gates versus Δ_B and g in a circuit with direct qubit-qubit coupling. The dashed lines correspond to the parameter regime for implementing two-qubit gate with fidelities 95% and 99.5%. The system parameters are the same as in Fig.6 except for $\Delta_A = \Delta_B$ for panel (a).

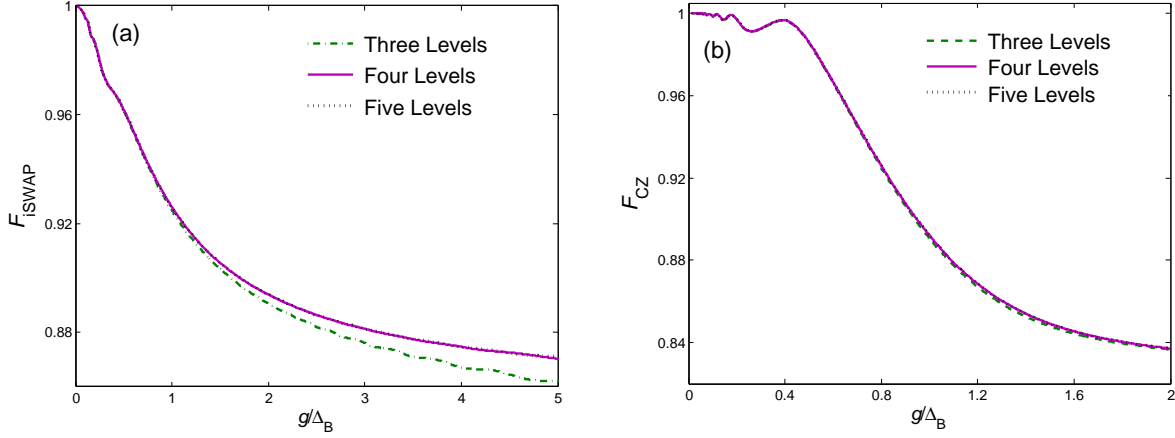


FIG. 10: (Color online) The fidelities of the two-qubit iSWAP gate (a) and the CZ gate (b) as a function of g/Δ_B in circuit with direct qubit-qubit coupling, when the superconducting qubits have three, four, or five levels. The system parameters are the same as in Fig. 6.

Figure 6(d) shows small oscillations in the fidelity of the two-qubit CZ gate. This result is due to the frequency mismatch between the undesired transitions and the resonant transition [see Figs. 3(b)], and the oscillations can be reduced by slowly adjusting the frequencies of the qubits during the gate operation. As shown in the inset of Fig. 7(a), the frequency of qubit B starts at $1.1\omega_B$, is first ramped down to ω_B in τ_d , then ramped up to $1.1\omega_B$ after an interaction time t_g ($\sqrt{2}gt_g = \pi$). During the full gate operation time ($2\tau_d + t_g$), the frequency of qubit A is fixed. Using such pulses, we numerically calculate the fidelities of the two-qubit CZ gate for different τ_d and present the results in Fig. 7. It can be seen from Figs. 7(a) and (b) that the oscillations in the high-fidelity regime can be eliminated by adiabatically adjusting the qubit frequencies during the gate operation.

In order to show the influence of Δ_A and Δ_B on the two-qubit gates, we plot the fidelities of the two-qubit iSWAP and CZ gates as functions of Δ_A/g and Δ_B/g in Fig. 8. It is easily seen from Fig. 8(a) that the anharmonicities Δ_A and Δ_B have equal effects on the two-qubit iSWAP gate, i.e., the larger the anharmonicities Δ_j ($j = A, B$) are, the higher the fidelity. This symmetric property disappears in the two-qubit CZ gate due to asymmetry in the condition on the parameters, $\omega_B = \omega_A + \Delta_B$ [see Fig. 8(b)]. In other words, the influence of the anharmonicity Δ_A on the two-qubit CZ gate can be neglected when $\omega_B = \omega_A + \Delta_B$ is chosen. In addition, the dashed lines in Fig. 8 indicate the safe regime of Δ_j/g ($j = A, B$) for implementing two-qubit iSWAP and CZ gates with fidelity higher than 99%.

1. *Changing both the coupling and the anharmonicity*

In Figs. 6 and 8, either the anharmonicity Δ_j or the coupling strength g have been set to a fixed value. A natural question is whether the conclusions obtained from Figs. 6 and 8 are universal. In other words, will the properties of Figs. 6 and 8 change much when either Δ_j or g is changed? Thus, we now present in Fig. 9 three-dimensional (3D) plots of the dependence of F_{iSWAP} (F_{CZ}) on g and Δ_B . It is shown these that the fidelity of two-qubit iSWAP and CZ gate are approximately determined by the ratio of the qubit-qubit coupling strength to the anharmonicity of the SC qubits. As a result, a similar conclusion will be obtained when Δ_B (or g) is changed in Fig. 7 (or Fig. 8).

2. *Beyond the three-level approximation*

Until now, all of the above numerical results were based on the same conditions. Namely that, each qubit was considered as a three-level system. It is then naturel to ask the following question: will our conclusions, obtained from the above numerical results, still be valid for qubits with N ($N > 3$) levels? To explore this, in Fig. 10, we plot the fidelities of the two-qubit iSWAP and CZ gates as functions of g/Δ_B when each qubit has three, four or five levels. It can be seen from Fig. 10 that there is not much difference (especially in the high-fidelity regime) between the numerical results based on the three-, four- and five-level approximations for the qubits. So, our conclusions obtained from the above numerical calculations are still valid for N -level (with $N > 3$) superconducting qubits.

B. **System with indirect qubit-qubit coupling**

In this subsection, based on the Hamiltonian (3), we present the results of numerical calculations for the dependence of the fidelity of the two-qubit gates on the effective qubit-qubit coupling g_{eff1} (or qubit-cavity coupling G) and anharmonicity of superconducting qubits Δ_j . Our numerical results in Figs. 11-14 agree with the qualitative conclusion in section II. Here the two-qubit CZ gates are realized based on the qubit-cavity dispersive interaction method [16] and resonant interaction method [34]. All the parameters used in the following numerical calculations are consistent with those methods, and $g_{\text{eff1}} = \frac{G^2}{2}(\frac{1}{\delta_B - \Delta_B} + \frac{1}{\delta_A}) = \frac{G^2}{\delta_A}$ under the condition $\omega_B = \omega_A + \Delta_B$.

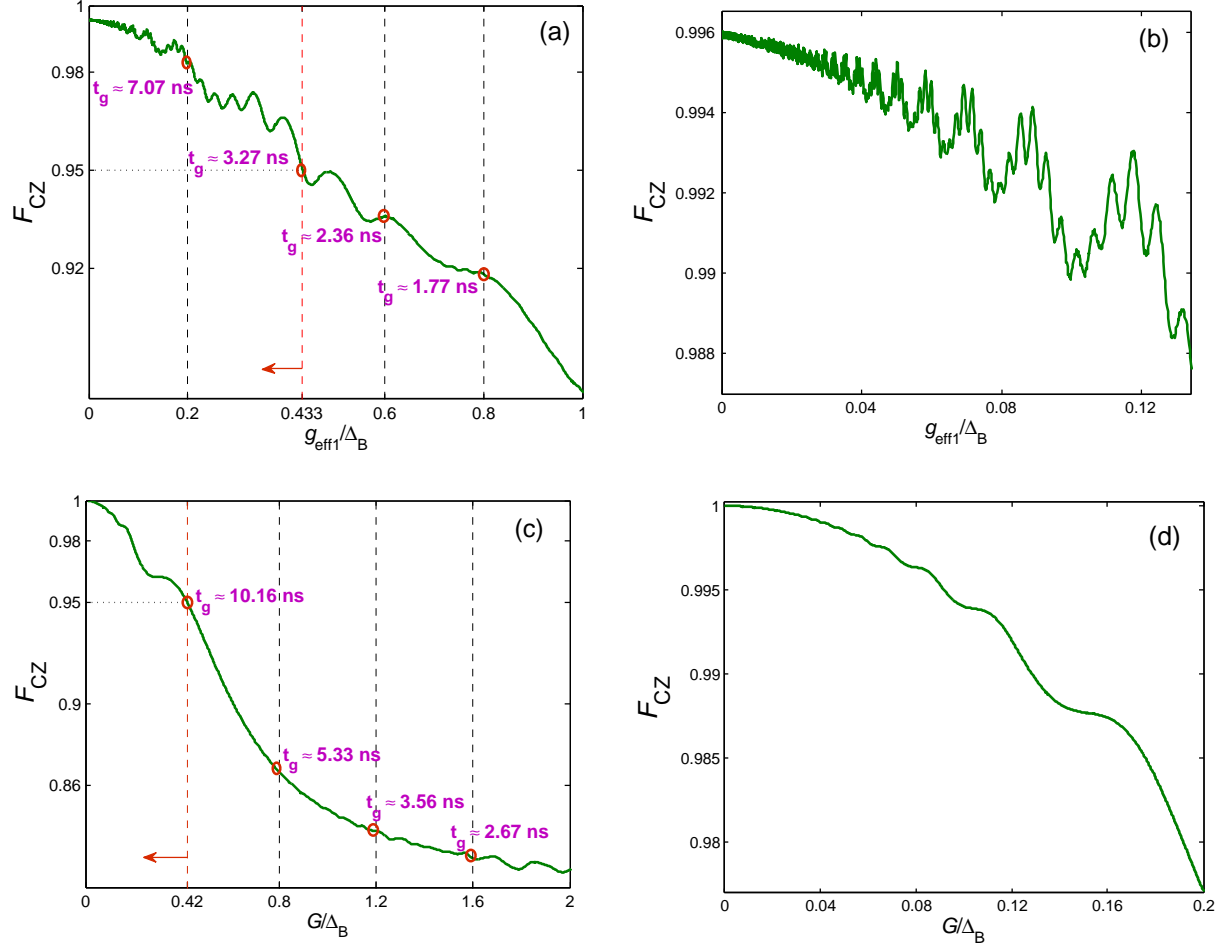


FIG. 11: (Color online) The fidelity of the two-qubit CZ gate as a function of g_{eff1}/Δ_B in the dispersive (a), (b) and G/Δ_B in the resonant (c), (d) qubit-cavity-coupling scheme. In figures (a) and (c), some representative dots are denoted by dashed lines and red circles, which present the relationship between the gate time and fidelity. The red arrows indicate the parameter regime corresponding to a two-qubit gate fidelity higher than 95%. In figures (b) and (d), we plot the high-fidelity parts of (a) and (c). The system parameters are: (a), (b) $\omega_c/2\pi = 6.9 \text{ GHz}$, $\omega_A/2\pi = 8.2 \text{ GHz}$, $\Delta_A/2\pi = 0.2 \text{ GHz}$, $\Delta_B/2\pi = 0.25 \text{ GHz}$; $\omega_B = \omega_A + \Delta_B$, $\delta_j = \omega_j - \omega_c$ ($j = A, B$). (c), (d) $\omega_c/2\pi = \omega_A/2\pi = 5 \text{ GHz}$, $\Delta_A/2\pi = 0.25 \text{ GHz}$, $\Delta_B/2\pi = 0.2 \text{ GHz}$, and $\omega_B = \omega_c + \Delta_B$.

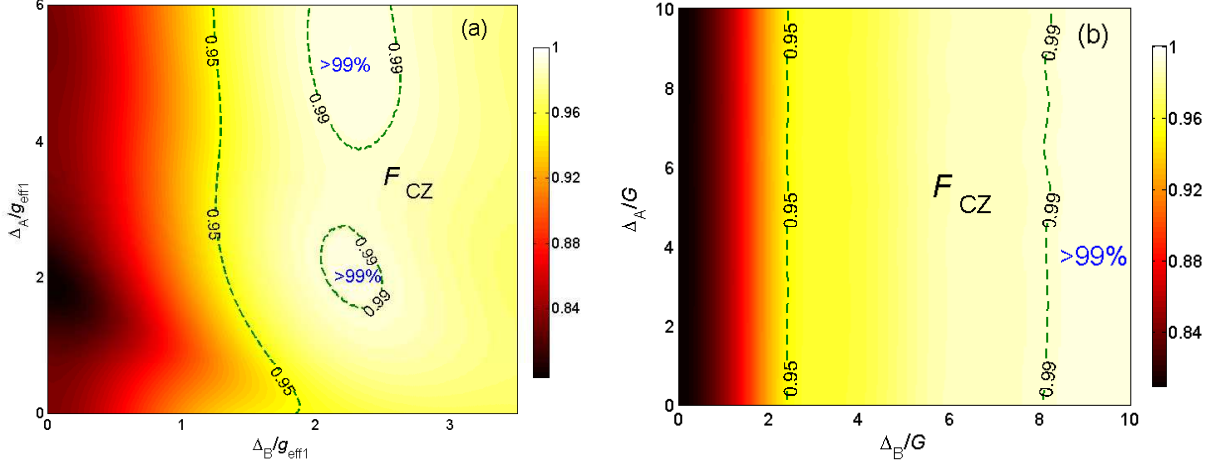


FIG. 12: (Color online) The fidelity F_{CZ} of the two-qubit CZ gate versus Δ_A/g_{eff1} , Δ_B/g_{eff1} in the dispersive (a), (b) and Δ_A/G , Δ_B/G in the resonant (c), (d) qubit-cavity-coupling scheme. The dashed lines correspond to the parameter regime for implementing two-qubit gate with fidelities 95% and 99%. The system parameters are the same as in Fig. 11 except for $G/2\pi = 0.2$ GHz.

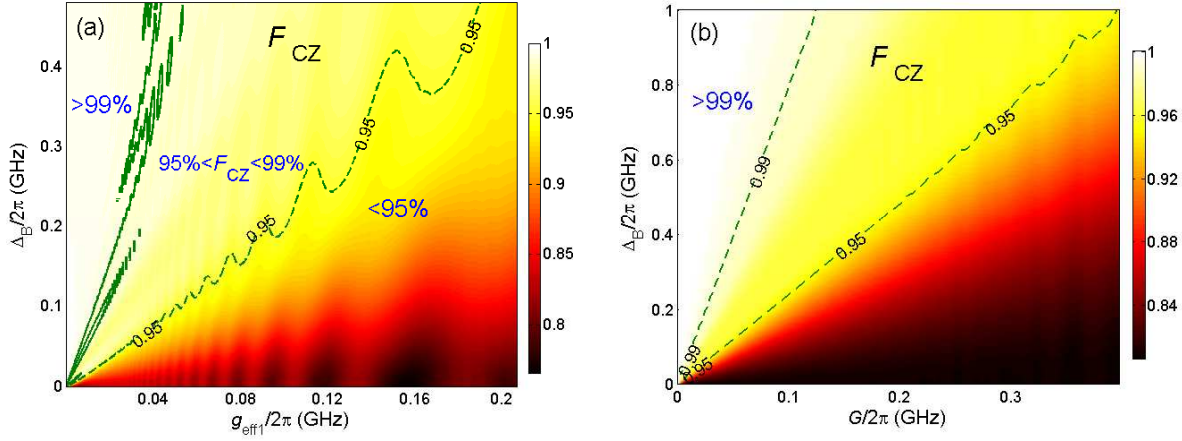


FIG. 13: (Color online) The fidelity F_{CZ} of the two-qubit CZ gate versus g_{eff1} , Δ_B in the dispersive (a), (b) and G , Δ_B in the resonant (c), (d) qubit-cavity-coupling scheme. The dashed lines correspond to the parameter regime for implementing two-qubit gate with fidelities 95% and 99%. The system parameters are the same as in Fig. 11.

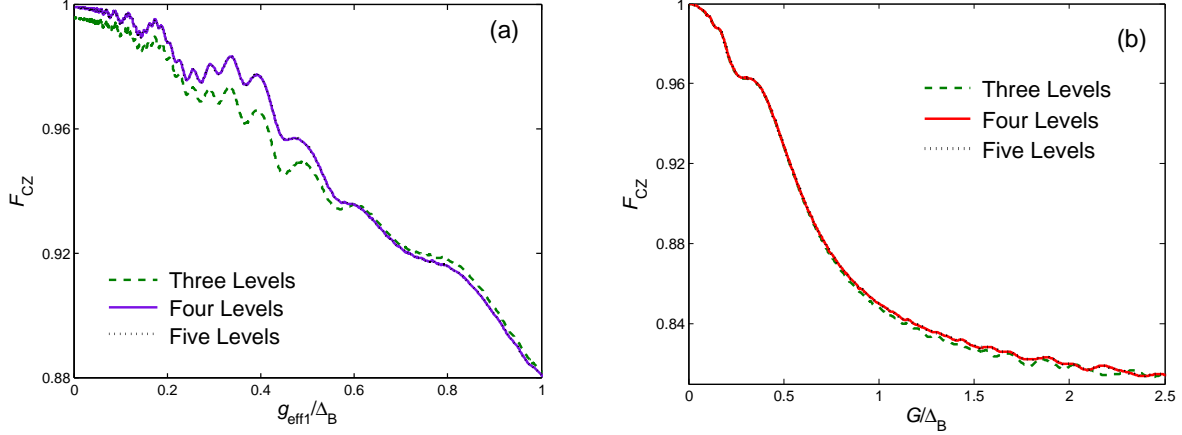


FIG. 14: (Color online) The fidelity of the two-qubit CZ gate as a function of g_{eff1}/Δ_B in the dispersive (a), (b) and G/Δ_B in the resonant (c), (d) qubit-cavity-coupling scheme, when the three, four, or five lowest levels are considered for each qubit. The system parameters are the same as in Fig. 11.

In Figs. 11(a) and (c), we plot the fidelity of the two-qubit CZ gate as functions of g_{eff1}/Δ_B (corresponding to the dispersive interaction approach) and G/Δ_B (corresponding to the resonant interaction approach) in a circuit with indirect qubit-qubit coupling, where we consider the superconducting qubits to have three levels (same approximation are used in Figs. 12 and 13). It can be seen from Figs. 11(a) and (c) that the fidelity of the two-qubit CZ gate decreases with increasing g_{eff1}/Δ_B or G/Δ_B . The present numerical results can be used to identify the safe parameter regime for implementing the two-qubit CZ gate with high fidelity. As shown in Figs. 11 (a) and (c), the safe parameter regime is $g_{\text{eff1}}/\Delta_B < 0.433$ ($G/\Delta_B < 0.42$) in order to implement the two-qubit CZ gate with fidelity higher than 95% in the dispersive (resonant) qubit-cavity-coupling method. Alternatively, the present numerical results can be used to identify the time limit for implementing the two-qubit CZ gate with high fidelity. For example, the shortest gate time is $t_g \approx 3.27$ ($t_g \approx 10.16$) ns for implementing the two-qubit CZ gate with fidelity higher than 95% in the dispersive (resonant) qubit-cavity-coupling method. Here the gate times are obtained using the relationships $\sqrt{2}g_{\text{eff1}}t_g = \pi$ for the dispersive qubit-cavity coupling method, and $Gt_{g1} = \pi/2$, $\sqrt{2}Gt_{g2} = \pi$, $Gt_{g3} = \pi/2$, $t_g = t_{g1} + t_{g2} + t_{g3}$, for the resonant qubit-cavity coupling method. In order to clearly show the dependence of the fidelity on g_{eff1}/Δ_B or G/Δ_B , in Figs. 11(b) and (d), we individually plot the high-fidelity parts of Figs. 11(a) and (c).

In Fig. 12, we plot the fidelity of the two-qubit CZ gate as a function of Δ_A/g_{eff1} and Δ_B/g_{eff1} (or Δ_A/G and Δ_B/G). Using dashed lines, we have denoted the parameter regime for implementing two-qubit CZ gate with fidelities 95% and 99%. It is shown that the fidelity of the two-qubit CZ gate decreases with increasing anharmonicity Δ_B , which is consistent with our qualitative discussion in section II. The safe regime of Δ_A and Δ_B for implementing the two-qubit CZ gate with fidelity higher than 99% is provided in this figure.

1. Changing both the coupling and the anharmonicity

In Fig. 13, we present 3D plots of the dependence of F_{CZ} on the coupling strength g_{eff1} (or G) and anharmonicity Δ_B . It is shown from Fig. 13(a) and (b) that the fidelity of the two-qubit CZ gate is approximately determined by the ratio g_{eff1}/Δ_B (or G/Δ_B); Moreover high fidelity corresponds to the weak-coupling regime $g_{\text{eff1}}/\Delta_B \ll 1$ (or $G/\Delta_B \ll 1$), while low fidelity corresponds to the strong-coupling regime, where g_{eff1} (or G) is comparable to or larger than Δ_B .

2. Beyond the three-level approximation

The three-level approximation for the superconducting qubits was used in the above numerical calculations (Figs. 11-13). In order to prove the validity of the above numerical results for $N > 3$, we plot the fidelity of the two-qubit CZ gate as a function of g_{eff1}/Δ_B (or G/Δ_B) in Fig. 14, where the three-, four- and five-level approximations are used for the qubits. It is shown that there is not much difference between the numerical results based on the three-, four-, and five-level approximations. So, the conclusion obtained from Figs. 11-13 is still valid for N -level qubits.

C. Maximum coupling strengths for implementing high-fidelity two-qubit gates

Before ending this section, based on the above numerical calculations, we present a table providing the maximum coupling strength for implementing two-qubit gates with high fidelity in the SC system (see Table I). In this table, we have set $\Delta_A/2\pi = \Delta_B/2\pi = \Delta/2\pi = 0.15$ GHz and the other parameters are the same as in Figs. 6 and 11. The methods I and

TABLE I: Maximum coupling strength for implementing two-qubit gates with high fidelity. Methods I and II correspond to the iSWAP and CZ gates in the circuits with direct qubit-qubit coupling, and methods III and IV correspond to the CZ gate in the circuits with dispersive and resonant qubit-cavity coupling.

	Direct qubit-qubit coupling		Indirect qubit-qubit coupling	
Fidelity	Method I (g/Δ)	Method II (g/Δ)	Method III (g_{eff1}/Δ)	Method IV (G/Δ)
99%	0.14	0.48	0.21	0.13
99.9%	0.04	0.14	0.05	0.04

II correspond to the iSWAP and CZ gates in the circuits with direct qubit-qubit coupling; while the methods III and IV correspond to the CZ gate in the circuits with dispersive and resonant qubit-cavity coupling. Here it should be pointed out that the present table is valid for general superconducting qubits, e.g., phase and transmon qubits.

IV. CONCLUSION

We have studied the performance of two-qubit gates in a system of two coupled superconducting qubits under the condition that the coupling strength is comparable to or larger than the anharmonicity of the qubits. First of all, by using the three-level approximation for the qubits, we analyzed and numerically calculated the dependence of the two-qubit gate fidelity on the qubit-qubit (or qubit-cavity) coupling strength and the anharmonicity of the qubits. Based on extensive numerical results, the safe parameter regime can be identified for implementing experimentally two-qubit gates with high fidelity. Secondly, we numerically calculated the fidelity of the two-qubit gates in the case of four- and five-level approximations for the qubits, and demonstrated the validity of our numerical results for N -level qubits with $N > 3$. Our results can serve as a guide for future experiments based on superconducting qubits.

Acknowledgments

AS and FN were partially supported by LPS, NSA, ARO, NSF grant No. 0726909, JSPS-RFBR contract No. 09-02- 92114, Grant-in-Aid for Scientific Research (S), MEXT Kakenhi on Quantum Cybernetics, and the JSPS via its FIRST program. XYL was supported by the National Natural Science Foundation of China under grant number 11005057.

- [1] J. Q. You and F. Nori, *Phys. Today* **58**(11), 42 (2005).
- [2] Y. Makhlin, G. Schön, and A. Shnirman, *Rev. Mod. Phys.* **73**, 357 (2001).
- [3] J. Clarke and F. K. Wilhelm, *Nature* **453**, 1031 (2008).
- [4] R. J. Schoelkopf and S. M. Girvin, *Nature* **451**, 664 (2008).
- [5] J. Q. You and F. Nori, *Nature* **474**, 589 (2011).
- [6] I. Buluta and F. Nori, *Science* **326**, 108 (2009).
- [7] I. Buluta, S. Ashhab, and F. Nori, *Rep. Prog. Phys.* **74**, 104401 (2011); T. D. Ladd, F. Jelezko, R. Laflamme, Y. Nakamura, C. Monroe, and J. L. O' Brien, *Nature* **464**, 45 (2010).
- [8] Y. Nakamura, Y. A. Pashkin, and J. S. Tsai, *Nature* **398**, 786 (1999).
- [9] C. H. van der Wal, A. C. J. ter Haar, F. K. Wilhelm, R. N. Schouten, C. J. P. M. Harmans, T. P. Orlando, S. Lloyd, and J. E. Mooij, *Science* **290**, 773 (2000).
- [10] J. M. Martinis, S. Nam, J. Aumentado, and C. Urbina, *Phys. Rev. Lett.* **89**, 117901 (2002).
- [11] J. Q. You, X. Hu, S. Ashhab, and F. Nori, *Phys. Rev. B*, **75**, 140515(R) (2007); M. Steffen, S. Kumar, D. P. DiVincenzo, J. R. Rozen, G. A. Keefe, M. B. Rothwell, and M. B. Ketchen, *Phys. Rev. Lett.*, **105**, 100502 (2010).
- [12] J. Koch, T. M. Yu, J. Gambetta, A. A. Houck, D. I. Schuster, J. Majer, A. Blais, M. H. Devoret, S. M. Girvin, and R. J. Schoelkopf, *Phys. Rev. A* **76**, 042319 (2007).
- [13] J. M. Martinis, S. Nam, J. Aumentado and C. Urbina, *Phys. Rev. Lett.* **89**, 117901 (2002); E. Lucero, M. Hofheinz, M. Ansmann, R. C. Bialczak, N. Katz, M. Neeley, A. D. O' Connell, H. Wang, A. N. Cleland, and J. M. Martinis, *Phys. Rev. Lett.* **100**, 247001 (2008).
- [14] R. C. Bialczak, M. Ansmann, M. Hofheinz, E. Lucero, M. Neeley, A. D. O'Connell, D. Sank, H. Wang, J. Wenner, M. Steffen, A. N. Cleland and J. M. Martinis, *Nature Physics* **6**, 409 (2010).

- [15] T. Yamamoto, M. Neeley, E. Lucero, R. C. Bialczak, J. Kelly, M. Lenander, M. Mariani, A. D. O'Connell, D. Sank, H. Wang, M. Weides, J. Wenner, Y. Yin, A. N. Cleland, and J. M. Martinis, Phys. Rev. B **82**, 184515 (2010); J. M. Chow, A. D. Córcoles, J. M. Gambetta, C. Rigett, B. R. Johnson, J. A. Smolin, J. R. Rozen, G. A. Keefe, M. B. Rothwell, M. B. Ketchen, and M. Steffen, Phys. Rev. Lett. **107**, 080502 (2011).
- [16] L. DiCarlo, J. M. Chow, J. M. Gambetta, L. S. Bishop, B. R. Johnson, D. L. Schuster, J. Majer, A. Blais, L. Frunzio, S. M. Givin and R. J. Schoelkopf, Nature **460**, 240 (2009).
- [17] R. Fazio, G. M. Palma, and J. Siewert, Phys. Rev. Lett. **83**, 5385 (1999).
- [18] M. Steffen, J. M. Martinis, and I. L. Chuang, Phys. Rev. A **68**, 224518 (2003).
- [19] Z. Zhou, S.-I. Chu, and S. Han, Phys. Rev. Lett. **95**, 120501 (2005).
- [20] P. Reberntrost, and F. K. Wilhelm, Phys. Rev. B **79**, 060507(R) (2009); F. Motzoi, J. M. Gambetta, P. Reberntrost, and F. K. Wilhelm, Phys. Rev. Lett. **103**, 110501 (2009).
- [21] A. Ferrón and D. DomÍnguez, Phys. Rev. B. **81**, 104505 (2010).
- [22] J. M. Gambetta, F. Motzoi, S. T. Merkel, and F. K. Willhelm, Phys. Rev. A **83**, 012308 (2011).
- [23] S. Ashhab and F. Nori, Phys. Rev. B **76**, 132513 (2007).
- [24] Y. X. Liu, L.F. Wei, J.S. Tsai, and F. Nori, Phys. Rev. Lett. **96**, 067003 (2006).
- [25] Y. Wu and X. Yang, Phys. Rev. B **76**, 054425 (2007).
- [26] Y. Wu and X. Yang, Phys. Rev. A **71**, 053806 (2005).
- [27] T. Yamamoto, M. Watanabe, J. Q. You, Yu. A. Pashkin, O. Astafiev, Y. Nakamura, F. Nori, and J. S. Tsai, Phys. Rev. B **77**, 064505 (2008).
- [28] F. W. Strauch, P. R. Johnson, A. J. Dragt, C. J. Lobb, J. R. Anderson, and F.C.Wellstood, Phys. Rev. Lett. **91**, 167005 (2003).
- [29] H. Fröhlich, Phys. Rev. **79**, 845 (1950).
- [30] C. P. Sun, Phys. Rev. D **41**, 1318 (1990).
- [31] H.R. Zhang, Y. B. Cao, Z. R. Gong, and C. P. Sun, Phys. Rev. A **80**, 062308 (2009).
- [32] S. Ashhab, A. O. Niskanen, K. Harrabi, Y. Nakamura, T. Picot, P. C. de Groot, C. J. P. M. Harmans, J. E. Mooij, and F. Nori, Phys. Rev. B **77**, 014510 (2008).
- [33] M. A. Sillanpää, J. I. Park and R. W. Simmonds, Nature, **449**, 438 (2007).
- [34] G. Haack, F. Helmer, M. Mariani, F. Marquardt, and E. Solano, Phys. Rev. B **82**, 024514 (2010).